

PAPER

Magnetostatically driven domain replication in Ni/Co based perpendicular pseudo-spin-valves

To cite this article: S M Mohseni *et al* 2016 *J. Phys. D: Appl. Phys.* **49** 415004

View the [article online](#) for updates and enhancements.

You may also like

- [Regulating the core/shell electric structure of \$\text{Co}_3\text{O}_4\$ @Ni-Co layered double hydroxide on Ni foam through electrodeposition for a quasi-solid-state supercapacitor](#)
Yuqiang Zhang, Yan Wang, Jiahui Zhu et al.
- [Study of \$\text{Ni}_{99}\text{-Co}_{07}\$ nanocrystalline electrodeposited alloy as anti-wear coating on mild steel substrate](#)
M Hamidouche, N Khennafi-Benghalem, S Jacomet et al.
- [The Sol-Gel-Derived Nickel-Cobalt Oxides with High Supercapacitor Performances](#)
Guangxia Hu, Chunhua Tang, Chunxiang Li et al.

ECS
The
Electrochemical
Society
Advancing solid state &
electrochemical science & technology

DISCOVER
how sustainability
intersects with
electrochemistry & solid
state science research

Magnetostatically driven domain replication in Ni/Co based perpendicular pseudo-spin-valves

S M Mohseni¹, M Hamdi¹, S Chung^{2,3}, S R Sani² and Johan Åkerman^{2,3}

¹ Department of Physics, Shahid Beheshti University, Evin, Tehran 19839, Iran

² Materials and Nanophysics, KTH Royal Institute of Technology, 164 40 Kista, Sweden

³ Department of Physics, University of Gothenburg, 412 96 Gothenburg, Sweden

E-mail: m-mohseni@sbu.ac.ir and majidmohseni@gmail.com

Received 29 June 2016, revised 18 August 2016

Accepted for publication 22 August 2016

Published 15 September 2016



Abstract

The effect of ferromagnetic layer thickness on the temperature-dependent stray-field-induced coupling mechanism is investigated in perpendicular pseudo-spin-valves based on $[\text{Ni}/\text{Co}]_5/\text{Cu}/\text{Co}-[\text{Ni}/\text{Co}]_n$ ($n = 2, 3, 4$, and 5). Experimental observations show that as n increases from 2 to 4, the difference in coercivity and anisotropy between the two ($[\text{Ni}/\text{Co}]_5$ or bottom-layer, and $[\text{Ni}/\text{Co}]_n$ or top-layer) layers increases and the room temperature coupling strength decreases. The coupling then increases for $n = 5$, as the coercivity difference shrinks and anisotropy decreases. At reduced temperature, the layers start to decouple at a temperature, which increases with n from 2 to 4 and decreases for $n = 5$ via a stray-field domain-replication mechanism. Our results are useful to control the coupling in pseudo-spin-valves for practical applications in magnetoresistive devices.

Keywords: spintronics, perpendicular spin valve, magnetostatic coupling, domain replication

(Some figures may appear in colour only in the online journal)

Introduction

Nanostructured magnetic multilayers (MLs) with perpendicular magnetic anisotropy (PMA) have attracted much attention for their potential applicability in spintronic devices [1, 2]. Ni/Co PMA MLs [3] in particular have become an interesting material in spintronics, since their PMA and unique magnetic properties can be readily tuned and controlled by varying the layer thicknesses, the number of ML repeats, and the seed layer [4–7]. Such MLs can also be combined with easy-plane materials, such as NiFe and CoFeB, to form tilted exchange springs with a high degree of additional anisotropy tunability [8–16]. Magnetic thin films with PMA are highly promising for applications in domain-wall electronics [17], spin wave based devices [18], spin-transfer torque (STT) elements (including spin-torque oscillators and STT-magnetoresistive random access memories [19–30]), and also recently in STT-driven magnetic droplet and dynamical skyrmion generators [31–39].

Among alternative state of the art of devices for STT effect, some are composed of two magnetic layers separated by a metallic or insulating spacer; these are known as spin valves or magnetic tunneling junctions, respectively. In such structures, the coupling between two magnetic layers must be taken into account [40–44] and minimized or controlled. Parasitic interactions can lead to malfunctioning, thus resulting in a lack of high yield output in the final device. Coupling mechanisms are classified into four different categories: (i) direct magnetic coupling through pinholes in the metallic or insulating spacer layer [45, 46], (ii) indirect exchange coupling via the Ruderman–Kittel–Kasuya–Yosida (RKKY) interaction [47], (iii) orange-peel (Néel) magnetostatic coupling [48–50] due to correlated roughness at both spacer interfaces, and (iv) magnetostatic coupling by stray-field [40, 41, 48, 51–55]. The last of these is most significant when the magnetic layers are in a multi-domain state, or when the lateral size of the structure is reduced [51–53]. This coupling thus plays an important role in structures including PMA MLs, as they

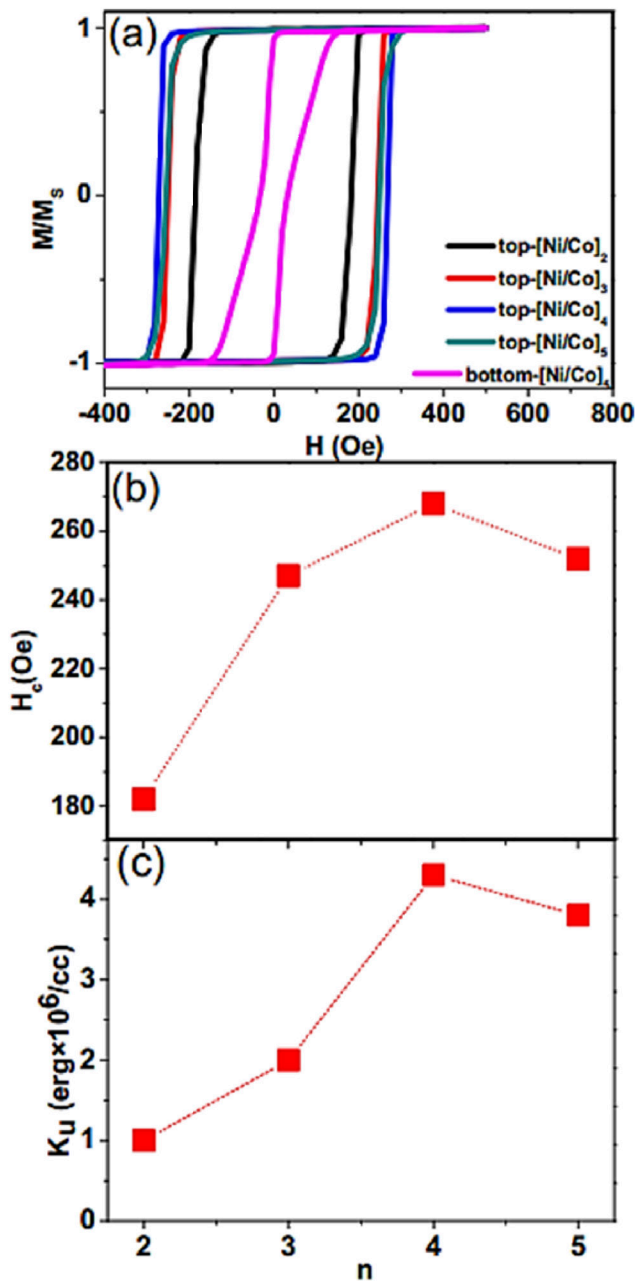


Figure 1. (a) Room temperature hysteresis loops for isolated top and bottom layers; (b) coercivity of isolated top layers determined from hysteresis loops and (c) PMA for isolated top layers.

show well defined multidomain states with large stray-field [40, 41, 48, 51–58]. For example, it has previously been shown that, in the presence of magnetostatic stray-field coupling, the remanent magnetization of one layer can be progressively reduced by the repeated switching of another layer [59], the nucleation field of layers can be decreased [60], magnetic domains of one layer can be replicated to another layer [61, 62], and asymmetric magnetization reversal can be achieved [40, 41]. Nevertheless, several solutions can be suggested to prevent domain replication in PMA spin valves. These include increasing the spacer-layer thickness—despite the fact that this results in a significant and undesirable reduction in the giant magnetoresistance (GMR)—and manipulating the

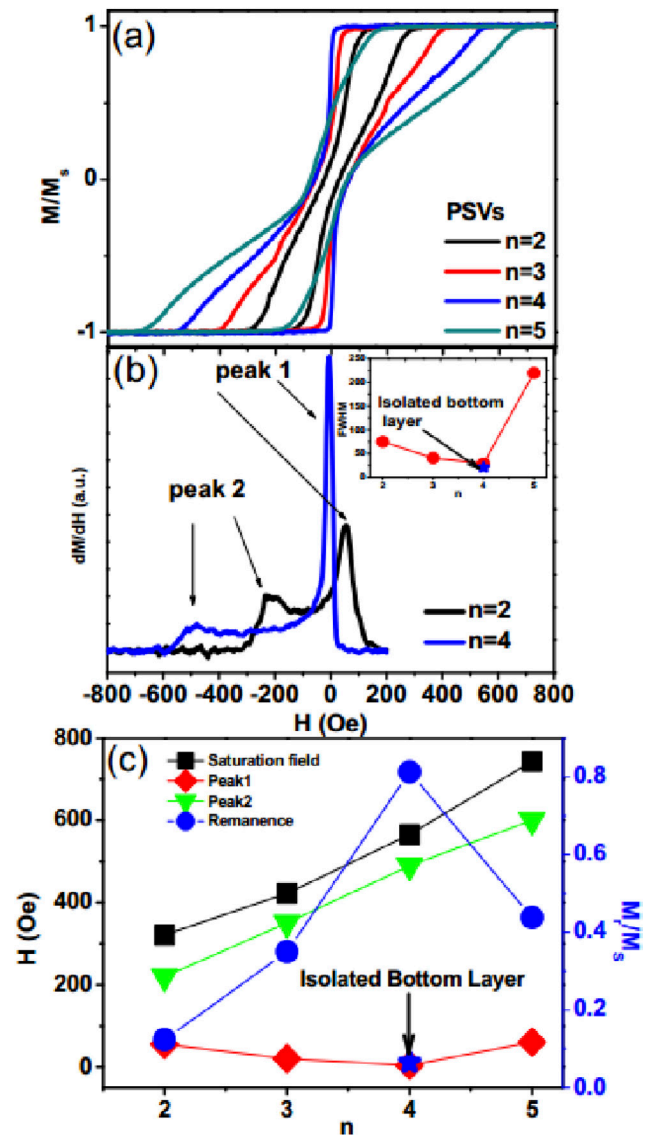


Figure 2. (a) Room temperature perpendicular hysteresis loops for PSVs with various n ; (b) derivative of descending hysteresis loop branch of PSVs, inset shows the FWHM determined from the peak 1 for various n ; (c) saturation field, peak position from derivative, and remanence from the magnetization loop of PSVs. The blue aster symbol in FWHM and peak1 position graphs indicate the FWHM and peak position for the isolated bottom layer respectively.

magnetic parameters of constitutive magnetic layers, such as the coercivity and anisotropy [41, 54, 63–70].

Recently, we have shown [54, 55] that, by reducing the temperature and thereby changing the coercivity for various thicknesses of a Cu spacer in a Ni/Co pseudo-spin-valve (PSV), complete decoupling as independent and distinguishable switching of the constituent MLs of the PSV stack could be achieved. Additionally, the peak positions determined from derivative of hysteresis loops have represented similar trend to the coercivity of isolated layers by reducing the temperature and increasing the spacer thickness, consistent with a stray-field-induced coupling mechanism. We have also shown that different spacer layer thicknesses can change the decoupling temperature, T_{decouple} , which is the temperature at which the layers begin to decouple.

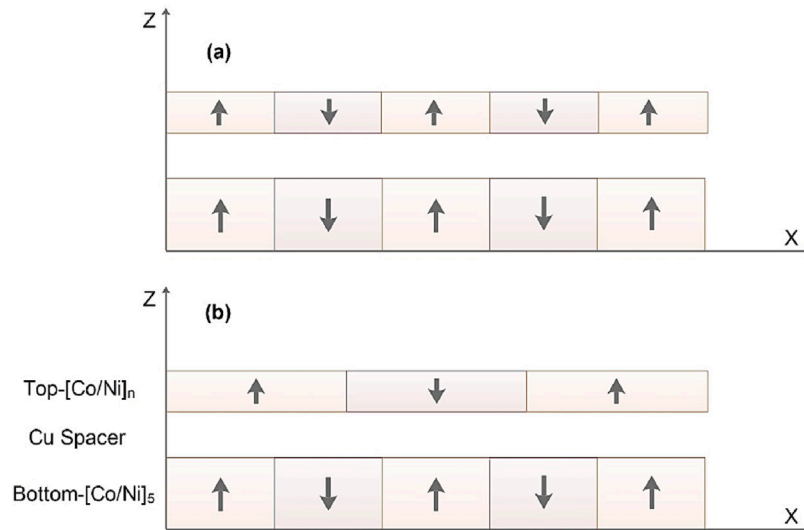


Figure 3. Definition of (a) replicated and (b) unreplicated energy states.

In this paper, we extend our previous findings [54] to systematically investigate the effect of ferromagnetic layer thickness on the temperature-dependent magnetostatic coupling in Ni/Co PSVs. We study the effect of top-layer thickness (i.e. ML repetition number, n) in the coupling mechanism of PSVs with the following structure: SiO₂/seed/[Ni/Co]₅/Cu/Co-[Ni/Co] _{n} /cap. Here, there are 4 different PSVs with a constant Cu spacer thickness of 6 nm, with a bottom-layer repetition number of 5, while the top-layer repetition number, n , varies incrementally from 2 to 5. As n increases, the magnetostatic stray field (proportional to $M_S \times$ thickness) increases, and the coercivity and anisotropy of the layers and their temperature-dependence differ. This allows studying the magnetostatic stray field coupling with stray field strength, anisotropy and coercivity of layers.

Experiments

All the film stacks were deposited at room temperature on thermally oxidized Si substrates using a magnetron sputtering system with a base pressure better than 5×10^{-8} Torr. The Ar process gas pressure was maintained at 5 mTorr for all layers. The sputtering rate for Ni, Co, and Cu were 0.19, 0.22, and 1.1 \AA s^{-1} , respectively. The full PSVs have the nominal layer structure [Ni(1)/Co(0.4)]₅/Cu(6)/Co(0.4)-[Ni(1)/Co(0.4)] _{n} , with all thicknesses in nanometers and the ML repetition number n varying from 2 to 5. In order to characterize the behavior of the individual MLs, Cu(6)/[Ni(1)/Co(0.4)] _{n} and [Ni(1)/Co(0.4)]₅/Cu(6) (thicknesses in nanometers), stacks were also deposited; these will simply be referred to as the isolated top-[Ni/Co] _{n} and bottom-[Ni/Co]₅ layers, respectively. Finally, all film stacks were deposited between a Ta (5 nm)/Cu (20 nm)/Ta (5 nm) seed and Ta (5 nm) capping layer.

Magnetic properties were characterized using a superconducting quantum interface device-vibrating sample magnetometer (SQUID-VSM) for variable temperature measurements, and an alternating gradient magnetometer (AGM) for room-temperature measurements.

Results and discussions

Effect of ferromagnetic layer thickness on room temperature coupling

Figure 1(a) shows the room temperature hysteresis loop of the isolated top-[Ni/Co] _{n} and bottom-[Ni/Co]₅ layers measured in a perpendicularly applied field. The coercivity determined from the major hysteresis loops, figure 1(a), for the top-layers is shown in figure 1(b). There is a clear increasing trend towards a maximum value for $n = 4$ and a slight reduction in coercivity for the $n = 5$ top-layer. This slight decrease may be due to the fact that the PMA degrades with increasing n for $n > 4$ [68], as it is determined from in-plane loop at room temperature, shown in figure 1(c). The anisotropy constant, as a function of n behaves in similar fashion to that for coercivity. Additionally, the coercivity for the bottom-layer is lower than for those deposited on the Cu spacer (top-layer), highlighting the important role of the underlayer [69]. The Cu spacer layer provides larger PMA for top layers as the Ni/Co stack favors similar crystallization of the Cu underlayer [69, 70].

Room temperature perpendicular hysteresis loops for the complete PSVs with various values of n are shown in figure 2(a). As we reported earlier [54, 55], the hysteresis loops for these structures are not simple superposition of the hysteresis loops of isolated top and bottom layers shown in figure 1(a). There is no clear indication of irreversible switching of top-[Ni/Co] _{n} layers in PSVs, whereas all of their isolated layers show a nearly perfect square-loop shape as shown figure 1(a). For all PSVs, as shown in figure 2(a), starting from a positive saturation field moving towards negative values, there is an immediate drop in magnetization at low fields, implying the domain nucleation. However, the domain nucleation responses in PSVs, shown in figure 2(a), appear to have different fashion to compare with those of either of isolated layers shown in figure 1(a). As shown in figure 2(b), the derivative (dM/dH) of descending trend of PSVs magnetization loop (for $n = 2, 4$), there are two peaks featured as peak 1 (low field) and peak 2 (high field) could correlate with domain

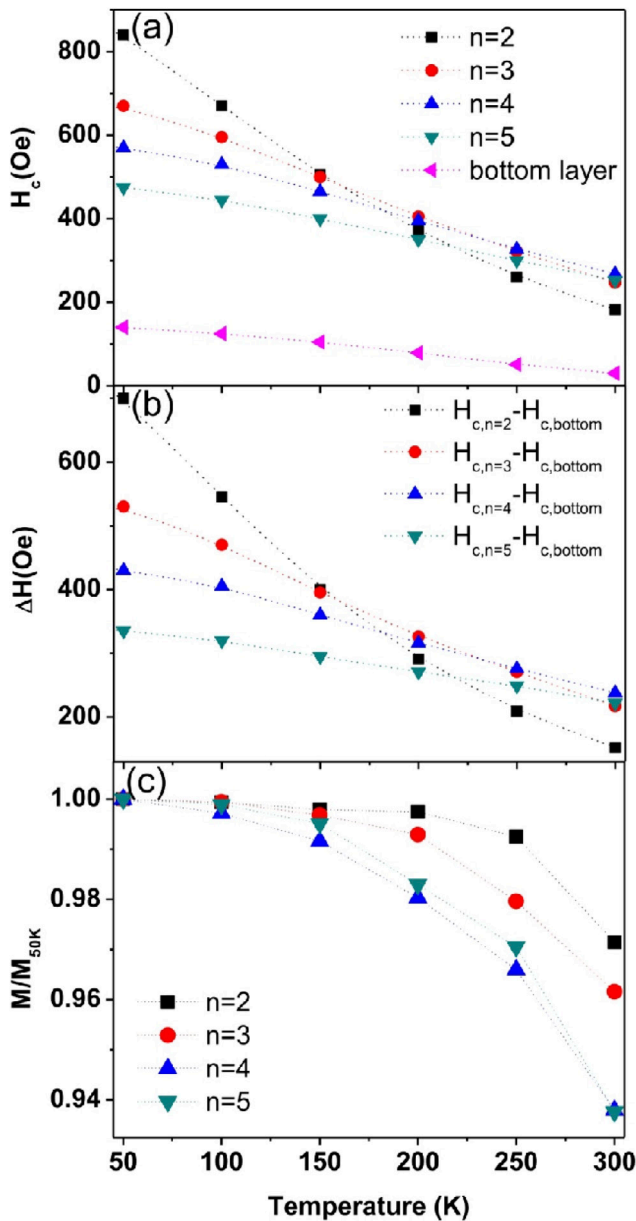


Figure 4. (a) Coercivity for isolated top and bottom layers as a function of temperature; (b) coercivity difference of isolated top and bottom layers; (c) saturation magnetization for isolated top layers measured in the presence of a 2000 Oe external field applied perpendicular to the samples.

nucleation in the presence of coupling for bottom-layer and top-layer in the PSVs, respectively. We note that such peaks do not correspond to the switching field of isolated bottom and top layers. In addition, the full width half maximum (FWHM) determined from peak 1 and the peak in hysteresis loop of isolated bottom-layer addresses the coupling field distribution of bottom-layer with and without coupling, respectively (inset of figure 2(b) for all PSVs and the blue aster for isolated bottom layer). This together with the derivative of magnetization can refer to coupling strength in the PSVs and suggests that the coupling strength decreases from $n = 2$ to $n = 4$ and increases thereafter. The FWHM value and peak position determined for $n = 4$ is very similar to the FWHM and peak position of the isolated bottom-layer (blue asters in the graphs

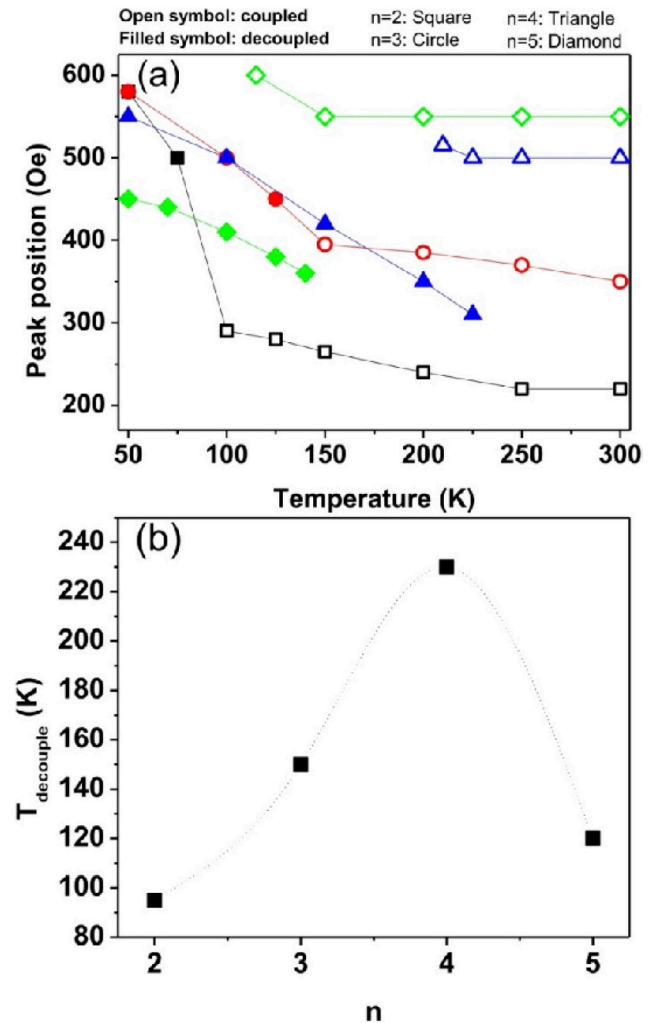


Figure 5. (a) Temperature-dependence of the major loop derivative peak 2 locations; (b) decoupling temperature versus repeating number n .

of figure 2(b) inset and figure 2(c)), as indication of the less coupled layers in the PSV. This can be already expected as the coercivity and anisotropy of isolated-top layer, figure 1(b), has the maximum value for $n = 4$ and, therefore, the stray-field of one layer hardly affects the magnetization reversal of another layer. Moreover, as shown in figure 2(c), peak 2 increases monotonously with n , whereas that for bottom-layer, peak 1, decreases from 55 Oe for $n = 2$ to a very low field of 4 Oe for $n = 4$, and then increases to 60 Oe for $n = 5$. The saturation field for the PSVs, figure 2(c), shows steady increase with n , whereas, the remanence value, figure 2(c), increases with n , and reaches a maximum value for $n = 4$ and that decreases for $n = 5$. Based on all above arguments, we therefore conclude that there is strong competition between the coercivity and anisotropy of top-layer and the stray-field emanating from the bottom-layer, which results in domain imprinting and vertically correlated domains [54, 55] (see schematic model of domain configuration in figure 3). The coercivity and anisotropy promote the stray-field coupling as n increases from $n = 2$ to $n = 4$ while stray-field dominates in the coupling for $n = 5$. This competition becomes clearer at reduced temperatures. Although the anisotropy of PSV with $n = 5$ is

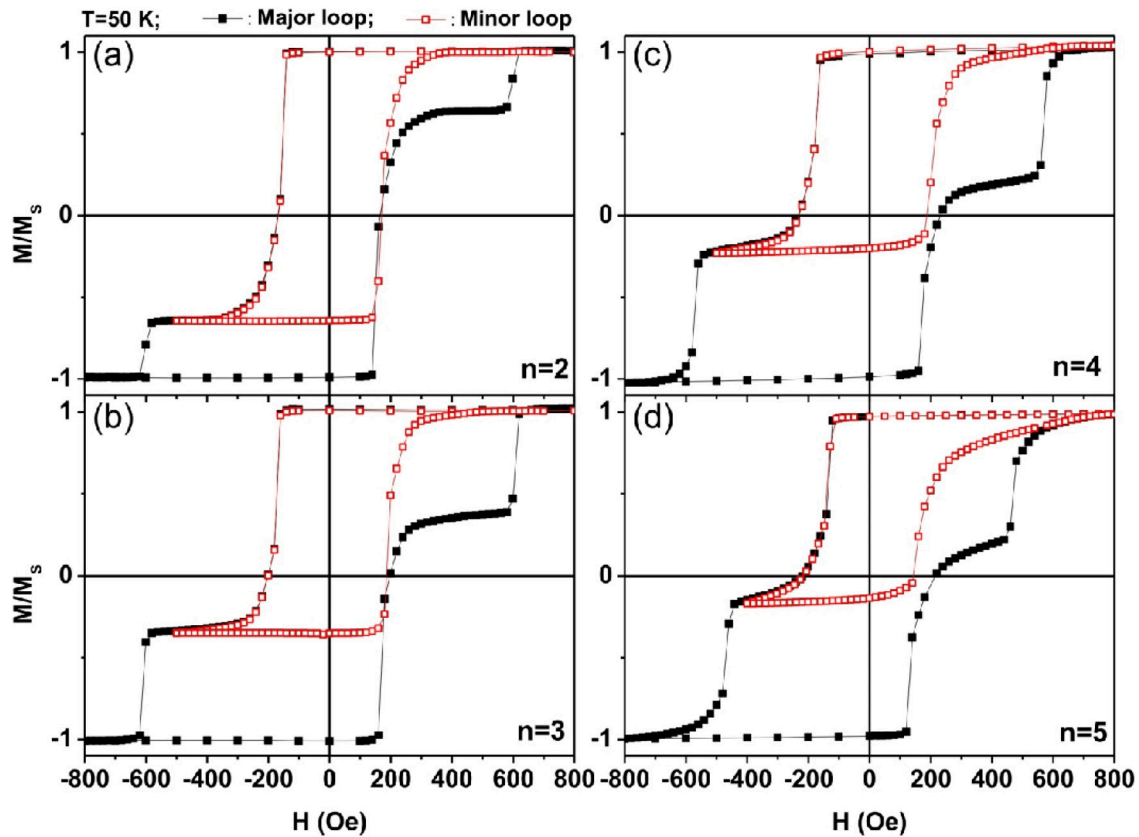


Figure 6. Perpendicular hysteresis loop of PSVs with $n = 2, 3, 4,$ and 5 ((a)–(d)), measured at 50 K, along with their reversal curves.

comparable to that PSV with $n = 4$, but it has larger thickness and hence there is larger magnetostatic coupling.

Effect of ferromagnetic layer thickness on low-temperature coupling

The temperature-dependent coercivity determined from the perpendicular hysteresis loops of the isolated top and bottom layers, is shown in figure 4(a). There is a dramatic increase in the coercivity of the top- $[\text{Ni}/\text{Co}]_n$ as the temperature is decreased. Similarly, it was already shown that the anisotropy increases dramatically when temperature decreases [54, 65, 66, 70]. Most importantly, the coercivity difference between the top and bottom layers, figure 4(b), increases at reduced temperatures with most significant rate for small n . Figure 4(c) shows the temperature-dependent saturation magnetization of the isolated top- $[\text{Ni}/\text{Co}]_n$ layers measured in the presence of a 2000 Oe external field applied perpendicular to the film plane and normalized to its value at 50 K. The ratio between the magnetization measured at 300 K and that at 50 K decreases with n . Additionally, the magnetization increases with decreasing temperature more rapidly for smaller n .

The temperature-dependent of peak 2 determined from the derivatives of the major hysteresis loops for all PSVs is shown in figure 5(a). The temperature where the layers begin to decouple is called T_{decouple} . We note that this statement does not mean that layers are necessary completely decoupled. In the temperature range below T_{decouple} , peak 2 shows trends very similar to those of the isolated top and bottom layers,

figure 4(a), similar to the observations in [54]. This range is indicated with solid symbols for all samples. PSVs with $n = 2$ and 3 represent a clear temperature range of coupling/decoupling whereas those with $n = 4$ and 5 show a complex response. Before layers start to decouple, their derivative maximum (peak 2) appears at high field (open symbol in figure 5(a)). By approaching T_{decouple} , peak 2 decreases dramatically, while continue to have steady increase with decreasing temperature, like those of isolated top layers (filled symbol in figure 5(a)). However, peak 1 does not show significant behavior (not shown) and increases with decreasing temperature below T_{decouple} . The result of determined T_{decouple} as a function of n is represented in figure 5(b). It is now straightforward to explain the role of n with coercivity and anisotropy in the coupling. By increasing n from 2 to 4, as the coercivity, anisotropy and the coercivity difference increases, T_{decouple} similarly increases. For $n = 5$, both layers have high saturation magnetizations and their coercivity difference does not increase with decreasing temperature; moreover, since they have the same domain size and same anisotropy, they require lower temperatures to reach larger anisotropies and larger coercivity differences to turn into a decoupled state. On the other hand, a slow temperature dependence of coercivity for $n = 4$ and 5 provides a wide range where layers are not completely decoupled. This hence requires a wider temperature range to reach a crucial coercivity difference to have layers decoupled.

To confirm the decoupling of the samples at reduced temperatures, a complete hysteresis loop and minor loop measured

immediately after saturation of the PSVs with $n = 2, 3$ and 4 , are shown in figures 6(a)–(c). These plots trace the reversal of the same portion of the bottom-[Ni/Co]₅ in the minor loop as well as distinguishable nucleation for constituent layers in the PSVs indicating completely decoupling of the PSVs at 50 K. However, the same plot for $n = 5$, shown in figure 6(d), does not show reversal of the same portion of magnetization in the minor loop, which implies that the top and bottom layers in this PSV are not completely decoupled at this temperature.

Conclusions

We have presented a detailed study of temperature-dependent magnetostatic coupling mechanisms as a function of ferromagnetic layer thickness in PMA PSVs. It was shown that by increasing the thickness of the ferromagnetic layers—and thus the stray field ($M_S \times$ thickness)—and also by varying the coercivity and anisotropy, there is competition between these parameters, which determines T_{decouple} . This temperature increases with room temperature anisotropy and coercivity for $n \leq 4$. For the highest room temperature anisotropy (at $n = 4$), despite the fact that saturation magnetization is high, the layers begin to decouple at higher temperatures.

Acknowledgments

Support from the Swedish Foundation for strategic Research (SSF), the Swedish Research Council (VR), and the Knut and Alice Wallenberg Foundation is gratefully acknowledged. S M Mohseni acknowledges support from the Iran National Science Foundation (INSF) and ISEF.

References

- [1] Ikeda S *et al* 2012 *SPIN* **2** 1240003
- [2] Sbiaa R, Meng H and Piramanayagam S N 2011 *Phys. Status Solidi RRL* **5** 413–9
- [3] Daalderop G, Kelly P and den Broeder F J 1992 *Phys. Rev. Lett.* **68** 682
- [4] Beaujour J-M, Ravelosona D, Tudosa I, Fullerton E E and Kent A D 2009 *Phys. Rev. B* **80** 180415
- [5] Beaujour J-M L, Chen W, Krycka K, Kao C-C, Sun J Z and Kent A D 2007 *Eur. Phys. J. B* **59** 475
- [6] Mizukami S, Zhang X, Kubota T, Naganuma H, Oogane M, Ando Y and Miyazaki T 2011 *Appl. Phys. Express* **4** 013005
- [7] Shaw J M, Nembach H T and Silva T J 2011 *Appl. Phys. Lett.* **99** 012503
- [8] Nguyen T N A, Fang Y, Fallahi V, Benatmane N, Mohseni S M, Dumas R K and Åkerman J 2011 *Appl. Phys. Lett.* **98** 172502
- [9] Chung S, Mohseni S M, Fallahi V, Nguyen T N A, Benatmane N, Dumas R K and Åkerman J 2013 *J. Phys. D: Appl. Phys.* **46** 125004
- [10] Nguyen T N A *et al* 2014 *Phys. Rev. Appl.* **2** 044014
- [11] Nguyen T N A, Benatmane N, Fallahi V, Fang Y, Mohseni S M, Dumas R K and Åkerman J 2012 *J. Magn. Magn. Mater.* **324** 3929
- [12] Nguyen T N A, Fallahi V, Le Q T, Chung S, Mohseni S M, Dumas R K, Miller C W and Åkerman J 2014 *IEEE Trans. Magn.* **50** 2004906
- [13] Tacchi S, Nguyen T N A, Gubbiotti G, Madami M, Carlotti G, Pini M G, Rettori A, Fallahi V, Dumas R K and Åkerman J 2014 *J. Phys. D: Appl. Phys.* **47** 495004
- [14] Morrison C, Miles J J, Anh Nguyen T N, Fang Y, Dumas R K, Åkerman J and Thomson T 2015 *J. Appl. Phys.* **117** 17B526
- [15] Tryputen L, Guo F, Liu F, Nguyen T N A, Mohseni S M, Chung S, Fang Y, Åkerman J, McMichael R D and Ross C A 2015 *Phys. Rev. B* **91** 014407
- [16] Escobar R A, Tryputen L, Castillo-Sepulveda S, Altbir D, Chung S, Nguyen T N A, Mohseni M, Åkerman J and Ross C A 2016 *IEEE Magn. Lett.* **7** 1
- [17] Boule O, Malinowski G and Kläui M 2011 *Mater. Sci. Eng. R* **72** 159
- [18] Gubbiotti G, Carlotti G, Tacchi S, Madami M, Ono T, Koyama T, Chiba D, Casoli F and Pini M G 2012 *Phys. Rev. B* **86** 014401
- [19] Mangin S, Ravelosona D, Katine J A, Carey M J, Terris B D and Fullerton E E 2006 *Nat. Mater.* **5** 210
- [20] Mangin S, Henry Y, Ravelosona D, Katine J A and Fullerton E E 2009 *Appl. Phys. Lett.* **94** 012502
- [21] Girod S, Gottwald M, Andrieu S, Mangin S, McCord J, Fullerton E E, J.-M. LBeaujour J-M L, Krishnatreya B J and Kent A D 2009 *Appl. Phys. Lett.* **94** 262504
- [22] Moriyama T, Finocchio G, Carpentieri M, Azzerboni B, Ralph D C and Buhrman R A 2012 *Phys. Rev. B* **86** 060411
- [23] Dieny B *et al* 2010 *Int. J. Nanotechnol.* **7** 591
- [24] Rippard W H, Deac A M, Pufall M R, Shaw J M, Keller M W, Russek S E, Bauer G E W and Serpico C 2010 *Phys. Rev. B* **81** 014426
- [25] Mohseni S M, Sani S R, Persson J, Nguyen T N A, Chung S, Pogoryelov Y and Åkerman J 2011 *Phys. Status Solidi RRL* **5** 432–4
- [26] Houssameddine D *et al* 2007 *Nat. Mater.* **6** 441
- [27] Stamps R L *et al* 2014 *J. Phys. D: Appl. Phys.* **47** 333001
- [28] Dumas R K, Sani S R, Mohseni S M, Iacocca E, Pogoryelov Y, Muduli P K, Chung S, Dürrenfeld P and Åkerman J 2014 *IEEE Trans. Magn.* **50** 4100107
- [29] Sani S, Persson J, Mohseni S M, Pogoryelov Y, Muduli P K, Eklund A, Malm G, Käll M, Dmitriev A and Åkerman J 2013 *Nat. Commun.* **4** 2731
- [30] Dumas R K, Iacocca E, Bonetti S, Sani S R, Mohseni S M, Eklund A, Persson J, Heinonen O and Åkerman J 2013 *Phys. Rev. Lett.* **110** 257202
- [31] Mohseni S M *et al* 2013 *Science* **339** 1295
- [32] Iacocca E, Dumas R K, Bookman L, Mohseni M, Chung S, Hofer M A and Åkerman J 2014 *Phys. Rev. Lett.* **112** 047201
- [33] Macià F, Backes D and Kent A D 2014 *Nat. Nanotechnol.* **9** 992
- [34] Mohseni S M *et al* 2014 *Physica B* **435** 84
- [35] Zhou Y, Iacocca E, Awad A A, Dumas R K, Zhang F C, Braun H B and Åkerman J 2015 *Nat. Commun.* **6** 8193
- [36] Xiao D, Liu Y, Zhou Y, Mohseni S M, Chung S and Åkerman J 2016 *Phys. Rev. B* **93** 094431
- [37] Chung S, Eklund A, Iacocca E, Mohseni S M, Sani S R, Bookman L, Hofer M A, Dumas R K and Åkerman J 2016 *Nat. Commun.* **7** 11209
- [38] Chung S, Majid Mohseni S, Eklund A, Dürrenfeld P, Ranjbar M, Sani S R, Nguyen T N A, Dumas R K and Åkerman J 2015 *Low Temp. Phys.* **41** 833
- [39] Chung S *et al* 2014 *J. Appl. Phys.* **115** 172612
- [40] Gottwald M, Hehn M, Lacour D, Hauet T, Moutafis F, Mangin S, Fischer P, Im M-Y and Berger A 2012 *Phys. Rev. B* **85** 064403
- [41] Hauet T and Hellwig O 2014 *J. Appl. Phys.* **115** 123911
- [42] Baltz V, Landis S, Rodmacq B and Dieny B 2005 *J. Magn. Magn. Mater.* **290–1** 1286
- [43] Samant M G and Parkin S S P 2004 *Vacuum* **74** 705
- [44] Albrecht M, Hu G, Moser A, Hellwig O and Terris B D 2005 *J. Appl. Phys.* **97** 103910

- [45] Wang J, Liu Y, Freitas P P, Snoeck E and Martins J L 2003 *J. Appl. Phys.* **93** 8367
- [46] van der Heijden P A A, Bloemen P J H, Metselaar J M, Wolf R M, Gaines J M, van Eemeren J T W M, van der Zaag P J and de Jonge W J M 1997 *Phys. Rev. B* **55** 11569
- [47] Teixeira J M, Ventura J, Fermento R, Araújo J P, Sousa J B, Cardoso S and Freitas P P 2008 *J. Appl. Phys.* **103** 07F319
- [48] Moritz J, Garcia F, Toussaint J C, Diény B and Nozières J P 2004 *Europhys. Lett.* **65** 123
- [49] Néel L and Hebd C R 1938 *Acad. Sci.* **49** 206
- [50] Néel L 1962 *C. R. Acad. Sci.* **255** 1676
- [51] Baltz V, Marty A, Rodmacq B and Diény B 2007 *Phys. Rev. B* **75** 014406
- [52] Krishnia S, Purnama I and Lew W S 2014 *Appl. Phys. Lett.* **105** 042404
- [53] O'Brien L, Petit D, Zeng H T, Lewis E R, Sampaio J, Jausovec A V, Read D E and Cowburn R P 2009 *Phys. Rev. Lett.* **103** 077206
- [54] Mohseni S M, Dumas R K, Fang Y, Lau J W, Sani S R, Persson J and Åkerman J 2011 *Phys. Rev. B* **84** 174432
- [55] Davies J E, Gilbert D A, Mohseni S M, Dumas R K, Åkerman J and Liu K 2013 *Appl. Phys. Lett.* **103** 022409
- [56] Fuller H W and Sullivan D L 1962 *J. Appl. Phys.* **33** 1063
- [57] Rodmacq B, Baltz V and Diény B 2006 *Phys. Rev. B* **73** 092405
- [58] Wiebel S, Jamet J-P, Vernier N, Mougín A, Ferré J, Baltz V, Rodmacq B and Diény B 2005 *Appl. Phys. Lett.* **86** 142502
- [59] Thomas L, Samant M and Parkin S 2000 *Phys. Rev. Lett.* **84** 1816
- [60] Vogel J et al 2005 *Phys. Rev. B* **72** 220402
- [61] Huet T, Günther C M, Pfau B, Schabes M E, Thiele J-U, Rick R L, Fischer P, Eisebitt S and Hellwig O 2008 *Phys. Rev. B* **77** 184421
- [62] Lew W S, Li S P, Lopez-Diaz L, Hatton D C and Bland J A C 2003 *Phys. Rev. Lett.* **90** 217201
- [63] Vértesy G, Tomáš I, Püst L and Pačes J 1992 *J. Appl. Phys.* **71** 3462
- [64] Vértesy G, Tomás I and Vértesy Z 2002 *J. Phys. D: Appl. Phys.* **35** 625
- [65] Staunton J B, Szunyogh L, Buruzs A, Gyorffy B L, Ostanin S and Udvardi L 2006 *Phys. Rev. B* **74** 144411
- [66] Staunton J B, Ostanin S, Razee S S A, Gyorffy B L, Szunyogh L, Ginatempo B and Bruno E 2004 *Phys. Rev. Lett.* **93** 257204
- [67] Janicka K, Burton J D and Tsymbal E Y 2007 *J. Appl. Phys.* **101** 113921
- [68] Macià F, Warnicke P, Bedau D, Im M-Y, Fischer P, Arena D A and Kent A D 2012 *J. Magn. Magn. Mater.* **324** 3629
- [69] Shaw J M, Nembach H T and Silva T J 2010 *J. Appl. Phys.* **108** 093922
- [70] Posth O, Hassel C, Spasova M, Dumpich G, Lindner J and Mangin S 2009 *J. Appl. Phys.* **106** 023919